JOURNAL OF AIRCRAFT
Vol. 31, No. 6, November–December 1994

Experimental Investigation of the Flowfield About an Upswept Afterbody

Ronald J. Epstein,* Mario C. Carbonaro,† and F. Caudron‡
von Kármán Institute for Fluid Dynamics, Rhode-Saint-Genese 1640, Belgium

In general, the flowfield about the aft portion of an aircraft fuselage employing an upswept afterbody is complex and can have a detailed vortex structure. Directional pressure probe measurements show that the afterbody wake evolution is weakly dependent on the Reynolds number. Pressure taps are used to investigate the effect of base slant on the base pressure distribution. The base pressure distribution is found to increase along the upswept ramp in the freestream direction. Using oil flow visualizations general conclusions are drawn about the surface flow topology. Two distinct regions of flow separation are identified. An analytical model of the crossflow wake structure is developed from the experimental data. This model allows for conclusions to be drawn about the crossflow vortex structure and provides simple analytical expressions for the vorticity and swirl velocity distributions in the crossflow plane.

Nomenclature

D = fuselage diameter length scale
$d\mathbf{s}$ = differential displacement vector
L = length scale
P = pressure
P_{pt} = pressure at pressure tap
P_{stat} = static pressure
q_∞ = freestream dynamic pressure
Re = Reynolds number, $\rho vL/\eta$
r = magnitude of radial position vector
r_c = vortex core radius
$\mathbf{r}$ = radial position vector
S = Strouhal number
U_∞ = freestream velocity
v = scalar velocity
v_θ = swirl velocity
$\mathbf{v}$ = velocity vector
x, y, z = Cartesian coordinate directions
α = angle of incidence
Γ = circulation around a vortex
γ = free curve in space
δ = length scale
η = viscosity
ρ = density
ω = vorticity

Introduction

IN order to meet operational requirements and make the rotation phase of takeoff, it is necessary that the aft fuselage portion of a rear-loading cargo-type transport aircraft employ upsweep. The upswept portion of the fuselage resembles a slanted base on an axisymmetric body; however, the rear horizontal stabilizer complicates this idealized geometry by forming an aft fuselage structure sometimes referred to as a "beaver-tail." The performance of aircraft with this type fuselage design may be affected adversely by the interfering flowfields of the wing, undercarriage housings, and the upswept afterbody itself. In general, the rear fuselage cross sections are noncircular and arranged about a cambered upswept centerline. When this type of aerodynamic body is subjected to a uniform freestream, a complex flowfield is initiated by three-dimensional flow separations on the aft fuselage, and subsequent regions of separated flow. These considerations introduce complexities into the mathematical analysis of the system; consequently, the computation of the resultant aerodynamic forces and moments is excessively burdensome.[1,2] A full three-dimensional Navier-Stokes solution would be necessary in order to properly resolve the details of the flowfield.

The afterbody flowfield is very dynamic and can have detailed vortex structure. In general, the separated flow and the surface flow topology are nonlinear. As shown in Fig. 1, the separation regions on the surface of the upswept ramp portion of the fuselage result in a flowfield characterized by a pair of large counter-rotating vortices that convect far downstream. These vortices have the effect of inducing a significant crossflow in the Trefftz plane,[3] the plane that is normal to the freestream vector, as shown in Fig. 1. The crossflow can exhibit large velocities, and high levels of both vorticity and kinetic energy. No hard separation line can be easily identified on the fuselage surface.[4] This is unlike the highly vortical flowfield of a slender body at a high angle of attack, such as a missile or a delta wing, where a separation line can be

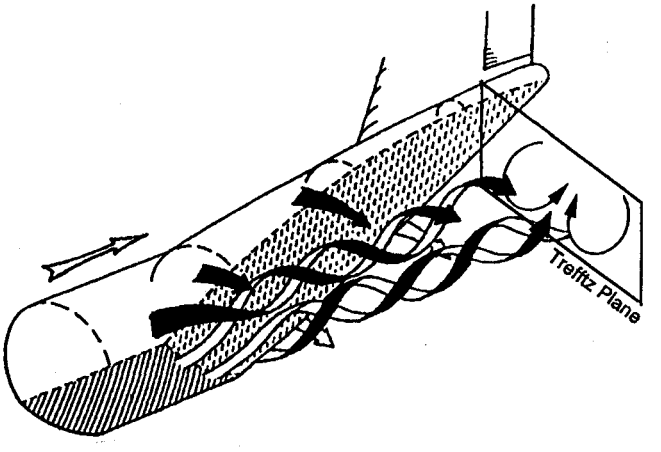

Fig. 1 Separation of trailing vortices from the upswept region of a fuselage afterbody.[14]

Received Nov. 21, 1993; revision received Feb. 23, 1994; accepted for publication Feb. 23, 1994.

*U.S. Air Force Research Fellow, Department of Aeronautics/Aerospace, 72 Chaussee de Waterloo; currently at Duke University, Department of Mechanical Engineering and Materials Science, Box 90300, Durham, NC 27708. Member AIAA.

†Professor, Department of Aeronautics/Aerospace, 72 Chaussee de Waterloo.

‡Research Fellow, Department of Aeronautics/Aerospace, 72 Chaussee de Waterloo.

identified in general for most cases. As a result, each aircraft geometry must be evaluated individually.

The upswept afterbody flowfield is fundamentally different from the classical aerodynamic problem of flow about a nonlifting body. This is sometimes referred to as the thickness problem. In the present work, the upswept afterbody exhibits a flow separation, and sheds a vortex wake. This wake phenomenon is created by the three-dimensional separation induced by the appropriate levels of viscous and inertial characteristics of the flow. Specifically, this wake is nonlift related insofar as it is not directly related to the bound circulation on the wing; it is only the circulation shed from the separation region, much like the wake shed from a bluff body. However, the vortex structure of this wake can produce an integrated negative lift effect on the upswept afterbody. Again, trying to model this flow as that about a bluff body would be ultimately unsuccessful, because there are considerable differences between both flowfields. The afterbody wake, in general, does not fluctuate with the regular rhythms corresponding to a Strouhal frequency, as does the von Kármán vortex street shed by the bluff body. The afterbody wake sheds symmetrically about the fuselage centerline, much like that of a delta wing. Only in the limiting case of large upsweep angles can the fluctuating behavior of the bluff body wake be partially regained. As such, this limits the feasibility and application of flow separation control devices,[4] because they are primarily designed for separation regions that close again with a region of reattachment. Nevertheless, the afterbody wake can possess a great deal of recognizable structure and it can be wholly deterministic in some flight regimes.[1]

There is a net drag force associated with the afterbody wake. The drag force manifests itself as a modification in the integrated pressure distribution on the aircraft. Specifically, the drag arises because of reduced pressures on the lower aft surfaces of the fuselage. As such, a suction force is experienced on the upswept ramp. The drag force is proportional to the suction force times the cosine of the upsweep ramp angle.

In phenomenological terms, the cause of the modified pressure distribution is the considerable loss of flow energy in the form of rotational kinetic energy of the vortex structure in the wake. Since the fluid is nondissipative, within the approximations of classical aerodynamics, it can store energy in kinetic form only, therefore this work must ultimately show up as part of the total kinetic energy left in the wake of the aircraft. Considering this, the afterbody wake can become a factor in the overall vortex drag calculation by increasing the total downwash on the wing by an incremental amount, thereby increasing the induced drag and reducing the net lift. In other words, the afterbody vortex drag is purely wasted energy.

The magnitude of upsweep-induced drag depends on the specific geometry of the aircraft in question, and in particular on the degree of upsweep and on the afterbody cross-sectional shape. Thus, an aircraft like the Lockheed C-130, with rather important changes in surface curvature in the rear fuselage region, generates much stronger vortical wakes than an aircraft like the Lockheed C-141, characterized by a much more smooth surface curvature variation. For the case of a military transport aircraft, the afterbody shape with an upswept ramp can be accountable for an important fraction of the total drag. A 50% reduction of this drag could be feasible, and might represent a 5% total drag reduction.[4]

However, in order to increase the overall performance of such an aircraft with novel drag reduction techniques, it is important that the physics of the afterbody flowfield be correctly understood. In turn this should rely on an experimental determination of the complete three-dimensional velocity field in the afterbody wake. Measurements of such flowfields were conducted by a number of investigators,[1,4] by five-hole probe or three-dimensional laser Doppler velocimeter (LDV) techniques; however, a bibliography survey conducted at the von Kármán Institute in 1988 using the ESA-QUEST data base, showed that no comprehensive description was published. Indeed, most of the published data concerns correlations between overall afterbody drag, as a function of the afterbody upsweep and cross section shape, and are substantiated by oil flow visualization patterns of the three-dimensional separations on the body surface.

Therefore, an experimental research program, initiated at the von Kármán Institute in 1983 to describe the upswept wake flowfield, and directed to the optimization of the positioning of drag reducing strakes, was continued. Test cases of the C-130 and the C-141 aircraft, as well as schematic afterbodies (cylinders with slanted flat bases) were considered, and a number of investigations were conducted at the von Kármán Institute on partial aspects of the wake flow, using surveys with five-hole probes, a technique much simpler and more economical to implement than three-dimensional LDV.

These studies indicated the need for a more general approach to the problem, and this resulted in the present research program, aimed at analyzing the wake evolution in space, its dependence on afterbody shape and Reynolds number. Thus, choosing the Lockheed C-130 as a test bed, it was decided to conduct flowfield measurements in a number of longitudinally spaced wake cross sections, using five-hole probe techniques, for several model scales, at different velocities. These measurements were complemented by oil flow surface visualizations and surface pressure measurements.

Test Apparatus and Instrumentation

All experiments were performed in the L2A low-speed windtunnel facility at the von Kármán Institute. The tunnel is an open-circuit type, with an atmospheric exhaust. The inlet has a 0.567-m^2 cross section, and has a contraction ratio of 8:1, which permits a 0.3- × 0.3-m working test section. The level of turbulence intensity for the tunnel is less than 0.5% for a frequency bandwidth from 1 to 10 kHz.

Three-dimensional velocity measurements were taken with five-hole directional pressure probes. The five-hole pressure probe consists of five pressure sensing tubes, or probes, lying in two perpendicular planes with the line of intersection of the two planes passing through the central probe. A schematic sketch of a five-hole probe, typical of those designed and manufactured by the VKI Instrumentation Lab, is shown in Fig. 2. The individual probes, made of 0.3-mm-i.d. nickel alloy, were soft solder bonded together. Longitudinal soft solder fillets between the tubes were formed to acceptable aerodynamic geometry. The probe tip (Fig. 2) was carefully fabricated, with special attention paid to obtain axial symmetry of the probe nose; however, being handmade, there are minute misalignments of the tubes with the centerline of the probe, as well as a certain degree of asymmetry of the nosetip. Therefore, an individual calibration of each probe is necessary.

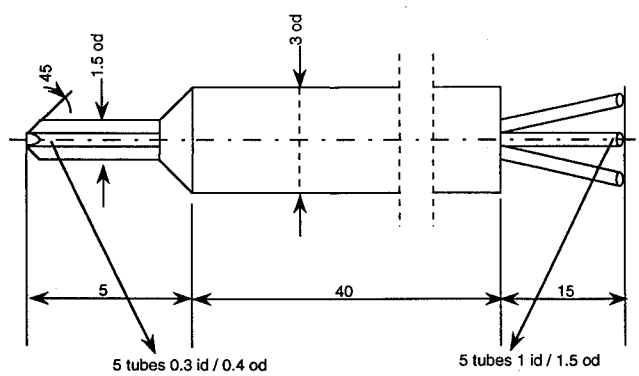

Fig. 2 Schematic sketch of a five-hole probe, typical of those designed and manufactured at the von Kármán Institute (all measurements in millimeters).

The data acquisition chain used was controlled by a personal computer with a high-speed data acquisition board. The scanning valve system, pressure measurement system, and the wind-tunnel traversing mechanism were fully computer automated to assure accuracy and consistency. In operation, the probe was manually set in a starting position in the traverse plane, with great care given to the probe alignment. The probe was aligned to the calibration axis using a leveling device that was accurate to within one-half deg of pitch and yaw. Each data acquisition cycle consisted of a pressure reading sequence, and a computer-triggered relocation of the probe. Once repositioned, the transients in the pressure lines were given time to damp, and a new cycle would begin. The data acquisition cycles continued until the probe reached a specified destination location. As such, the probe location was known to within one-fifth a measurement grid spacing.

The conversion from analog to digital was taken care of by the A/D converter of the data acquisition board. The final pressure acquisition was an average of 2000 samples. The sampling frequency of the data acquisition system was 4096 Hz; therefore, the maximum frequency resolved without aliasing was 2048 Hz. The unsteady fluctuations in the pressure signal varied over 10 or 11 complete cycles during a period of 0.2 s, hence, the 0.48-s sampling period seemed ample to give a good time-averaged signal.

The five-hole probe methodology is relatively simple and quite effective for three-dimensional velocity measurements. For the sake of brevity, only a brief description of the method will be given here. For an in-depth description of the five-hole probe methodology, the reader is referred to Refs. 5 and 6.

The five-hole probe methodology is based on the observation that the response of a stagnation pressure probe varies as a function of its relative freestream misalignment angle. Therefore, if a larger probe consisting of multiple smaller probes is oriented in such a way that the pressure differentials experienced between the individual smaller probes varies uniquely within the domain of angular measurement, a calibration map can be deduced that relates the misalignment angle of the larger probe to the respective pressure differentials in the multiprobe subsystem. The calibration maps give the one-to-one relationship between probe angular position and the defined pressure differential parameters. In fact, it is possible to define the pressure differential parameters, known as the calibration parameters or angular response functions, in such a way that they are independent of the local Reynolds number.[5,6] Once the angular response functions are determined, the flowfield can be wholly deduced by immersing the probe in the measurement stream, and back solving for the relative flow angles. The static pressure and the stagnation pressure can be determined in much the same manner, by defining angular functions that describe the dynamic pressure as a function of probe angular position in an oncoming freestream.

During the calibration process, the probe position is varied with respect to the experimental frame of reference; normally, one would prefer to align the experimental frame with the longitudinal coordinate of the freestream. Relationships can then be determined between the measured parameters at the five sensing probes and the true local values of total pressure, static pressure, and flow direction.[5,6] The nondimensionalized calibration parameters represent the pressure differences in both the pitch and yaw planes, independent of Reynold's number. The flow angles are defined using the standard aircraft convention: looking into the freestream, positive pitching up, and positive yaw to the right.

To conduct the calibration properly, a special pitch-yaw device was built that enabled the rotation of the probe in the pitch and yaw directions, while the probe-nosetip was kept at a constant spatial location. As such, only the tail portion of the five-hole probe was moved. This system was then mounted in the working section of a wind tunnel and the test section dynamic pressure was maintained at 35 mm H_2O. The probe was positioned at an initial yaw angle and then rotated in increments of 5 deg through the pitch range (-40 deg $\rightarrow$ $+40$ deg). At each of the calibration points, the relevant pressures were measured. Then the yaw angle orientation was incremented by 5 deg to a new value, and the entire procedure was repeated once again, from the beginning pitch angle, until the final yaw angle was reached (-40 deg $\rightarrow$ $+40$ deg). Once the calibration maps were completed, measurements could be taken. During measurements, constant monitoring of the position of the probe with respect to the rotation and tilt angles was needed in order to assure that misalignment velocities were not measured.

The Lockheed C-130 was chosen as a test bed for the flowfield measurements. The C-130 is a transport-style aircraft that has all of the characteristics previously discussed, and is therefore representative of large aircraft with an upswept afterbody. The upsweep angle of the C-130 is approximately 28

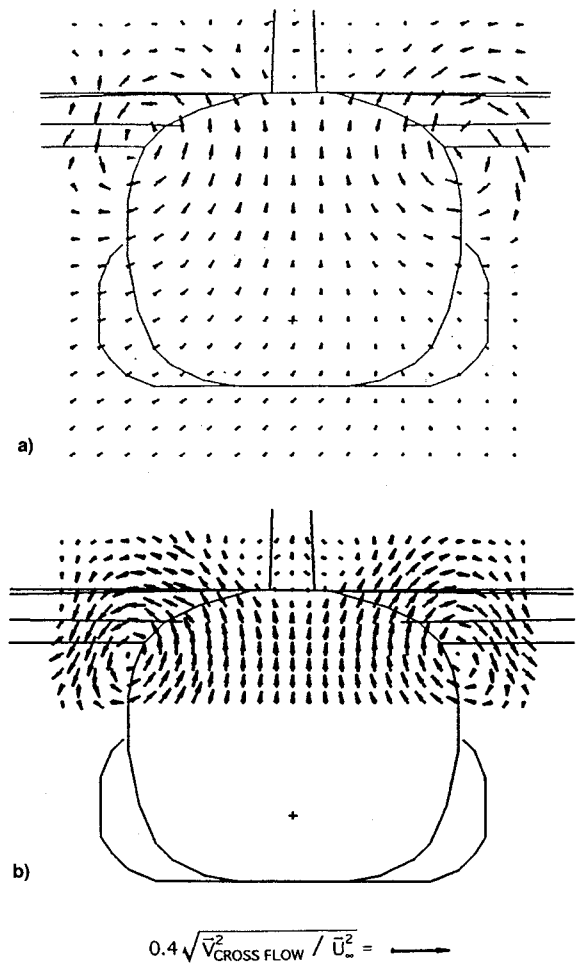

Fig. 3 Five-hole probe crossflow velocity measurements of the C-130 afterbody wake (x/D = 3.36, Re = 1.18 × 10^5). Grid spacing to fuselage diameter ratio of a) 12 and b) 20.

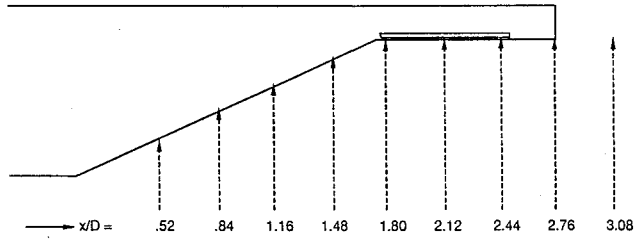

Fig. 4 Axial positions for five-hole probe traverses (not drawn to scale).

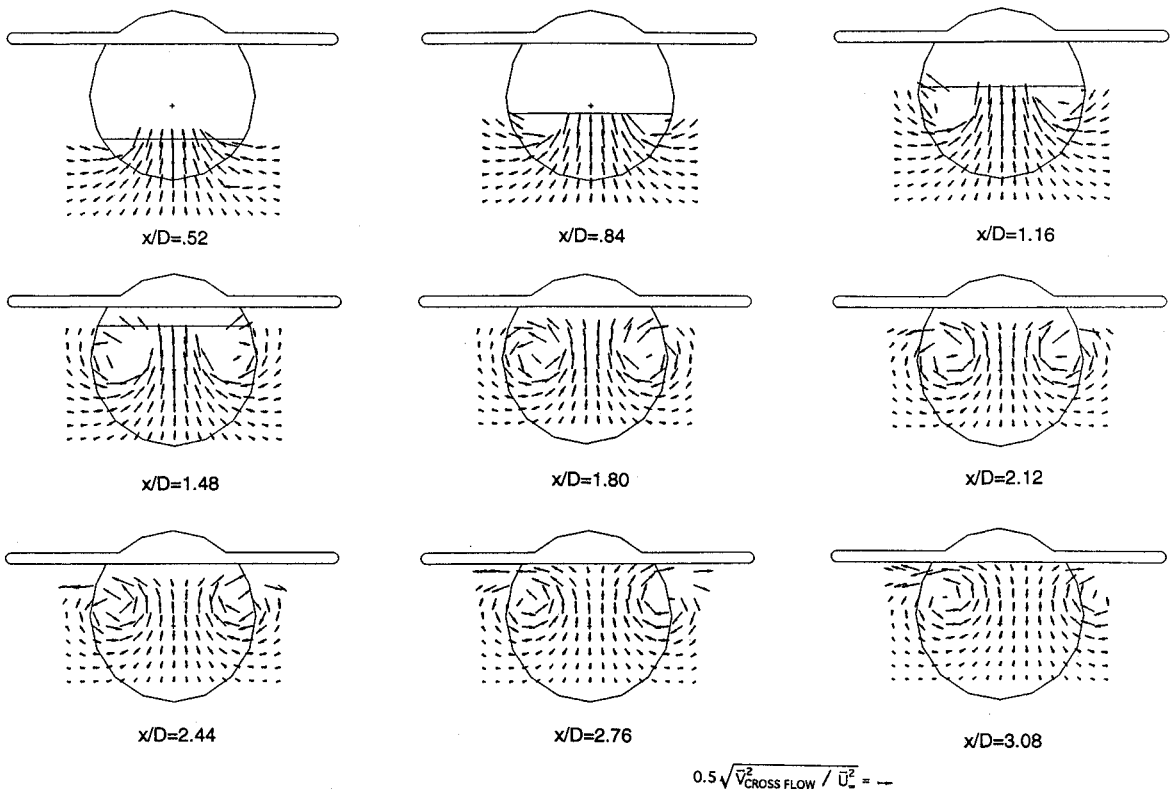

Fig. 5 Axial five-hole probe measurements depicting the wake evolution in the freestream direction at different x/D positions, $Re = 1.66 \times 10^5$.

deg. However, the reader should be aware that the C-130 was not chosen for any other reason than its fuselage style. There have been many different aircraft with upswept beaver-tail afterbodies produced internationally, and the C-130 is truly a generally representative fuselage test bed. It is the hope of the authors that the results presented in this article can give a better understanding of the afterbody aerodynamics in a more general sense than the specific test cases presented.

Three different C-130 models were constructed. Due to test-section size constraints, the tests had to be done at Reynolds numbers clearly below the actual flight Reynolds number, however, the results obtained correspond to the earlier results of Caudron[7] that were measured at more realistic Reynolds numbers. Two models were constructed at 1:32 scale. These two were precise C-130 models, but were modified in a specific manner. Both models had clipped wings in order to fit in the tunnel. Additionally, both models were built without a vertical stabilizer, and as such the beaver-tail was more isolated for testing. One model had wheel pods, whereas the other did not. The final model was an actual 1:72 scale model of the C-130. This model included all the fuselage characteristics, including wings, a vertical stabilizer, a horizontal stabilizer, and wheel pods. All the models were fabricated in the von Kármán Institute model shop.

Experimental Results and Discussion

Five-Hole Probe Results

Five-hole probe surveys were done in the wake of all the models at four Reynolds numbers: 8.3×10^4, 1.18×10^5, 1.66×10^5, and 2.37×10^5. The fuselage diameter was used as the characteristic length scale. The test runs were in the incompressible subsonic range. Throughout the research program, well over a hundred runs were recorded and representative results are being presented in this article. All of the work presented was done at a fixed fuselage angle of attack parallel to the oncoming freestream.

Each model tested shed a vortex wake from the upswept portion of the fuselage. The wake was characteristically dominated by two strong three-dimensional vortex structures emanating from a line or point of separation on the surface of the upswept ramp. The visualizations, like the ones shown in Fig. 3, confirm the expected circular shape of the trailing vortices in the crossflow plane. Note that the measurements in the lower portion of Fig. 3 were made with a fairly high-resolution grid, a grid-spacing-to-fuselage diameter ratio of 20, and it is possible to see the vortex core region. Whereas in the top portion a lower resolution was used in order to visualize a larger portion of the flowfield. The grid-spacing-to-fuselage diameter ratio used was 12.

The shape of the vortices did not seem to be a function of the test Reynolds number, nor was the position of the vortical core. The vortex flow was measured in the crossflow plane along various axial locations of the aircraft fuselage, Fig. 4 shows the axial measurement positions. Figure 5 shows measurements made along the fuselage axis and depicts the evolution of the wake in axial varying crossflow planes. The vortex core region is recognizable in all the plots. The position of vortex core center has been plotted in Fig. 6 as a function of axial position and is shown to be relatively constant and independent of Reynolds number. This is confirmed by the higher Reynolds number results of Caudron.[7] In fact, the position of the core was found to be the same for the model with wheel fairings as for the model without wheel fairings. However, this does not necessarily mean that the vortex structure of both flows remains the same as they convect downstream, but there is no obvious mechanism for why the flowfields might vary. In a simplified sense, the velocity field in the crossflow plane at one axial station is carried to the next axial location by convection with the freestream, while vortex induced velocities cause the flowfield to deform from the profile at the previous axial location. Globally, the vortices shed by the afterbody twist in a helicoidal fashion as they convect downstream, until they viscously disperse downstream of the fuselage.

Due to wind-tunnel constraints, relatively small Reynolds numbers were studied. Realistic Reynolds numbers would be

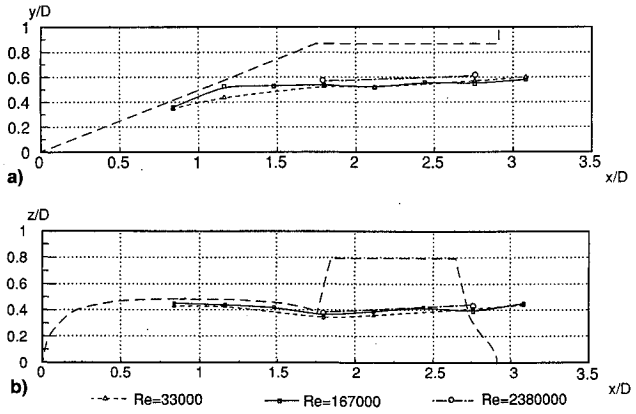

Fig. 6 Position of the vortex core center as a function of axial position and Reynolds number: a) side and b) top view.

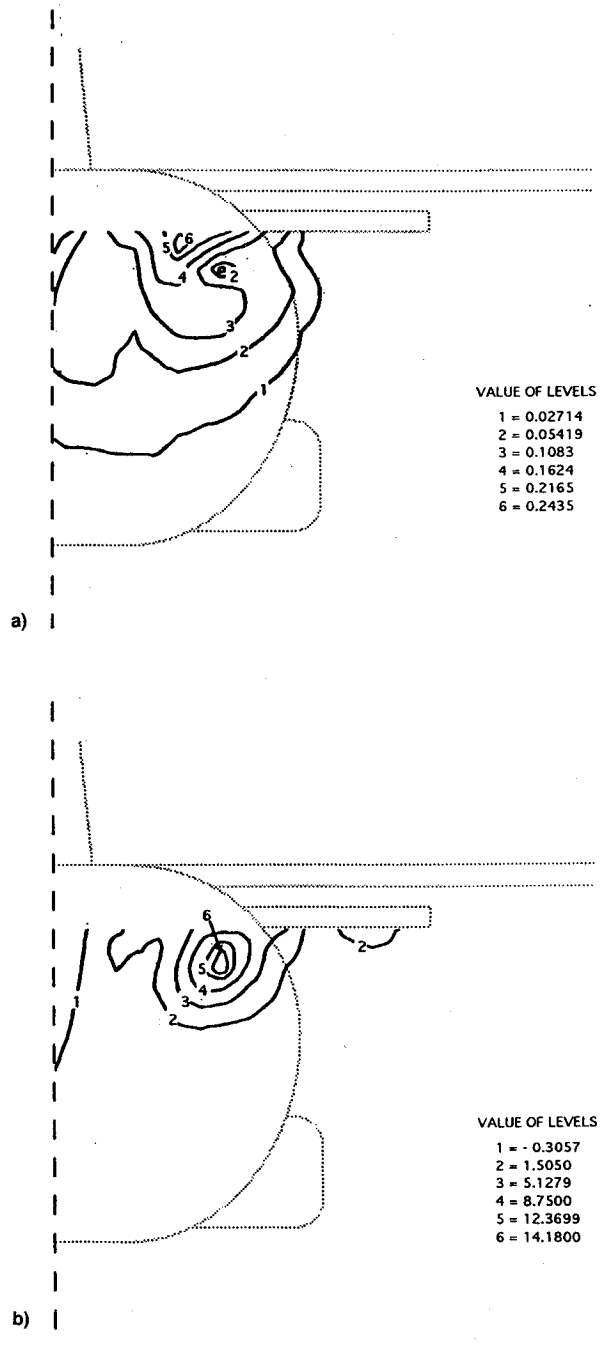

Fig. 7 Crossflow a) kinetic energy and b) vorticity contours in the C-130 afterbody wake (x/D = 2.12, Re = 1.66 × 10^5).

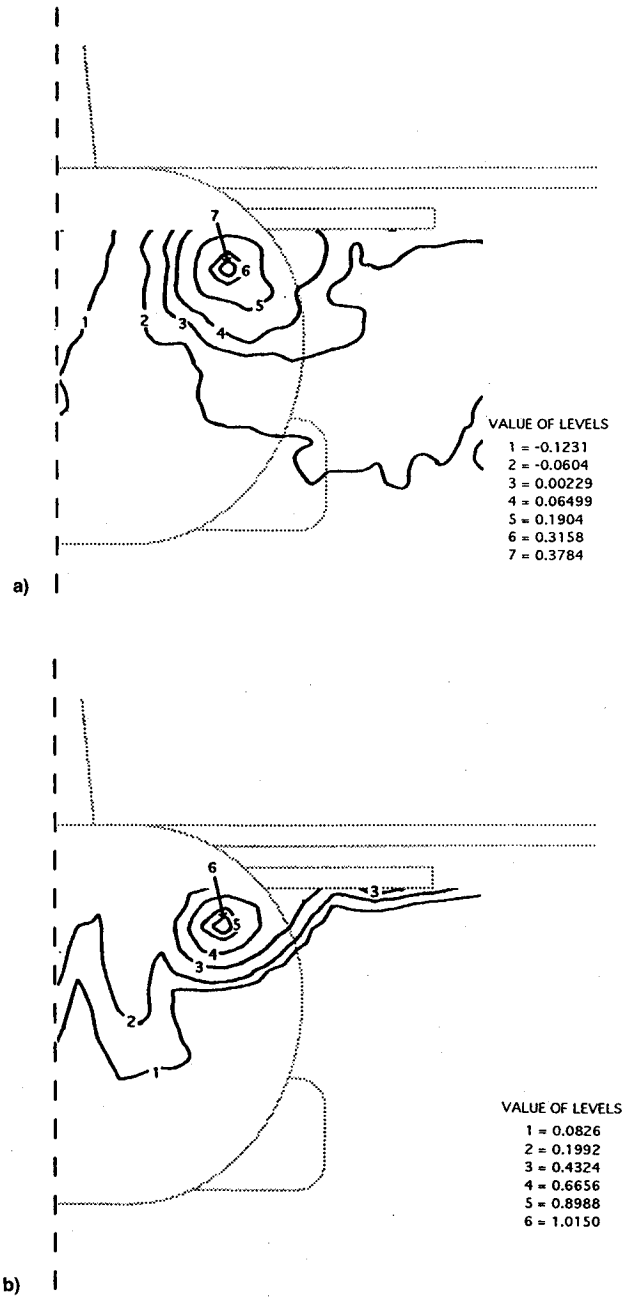

Fig. 8 a) Static pressure and b) total pressure contours in the C-130 afterbody wake (x/D = 2.12, Re = 1.66 × 10^5).

roughly one order of magnitude larger; however, no clear dependence on Reynolds number was observed in the results. Therefore, the vortex evolution appears to be, at most, weakly related to Reynolds number. This seems logical, as traditionally most wake structures are considered to be modeled as incompressible and inviscid flows.

The formation of the wake occurs when there is a three-dimensional boundary-layer separation on the upswept portion of the fuselage. Hence, once the wake actually separates from the fuselage it is free to convect downstream. Therefore, the major factors affecting the position of the vortex core of the wake is the separation point on the fuselage, the freestream, and the self-induced motion of the wake. Specifically, with this kind of wake structure, if the wake has a constant vortex core position at one location, it will have a constant vortex core position at all locations. This is provided that there are no obstructions in the downstream direction and the freestream does not vary, because the wake convects in a Lagrangian sense with the constant freestream.

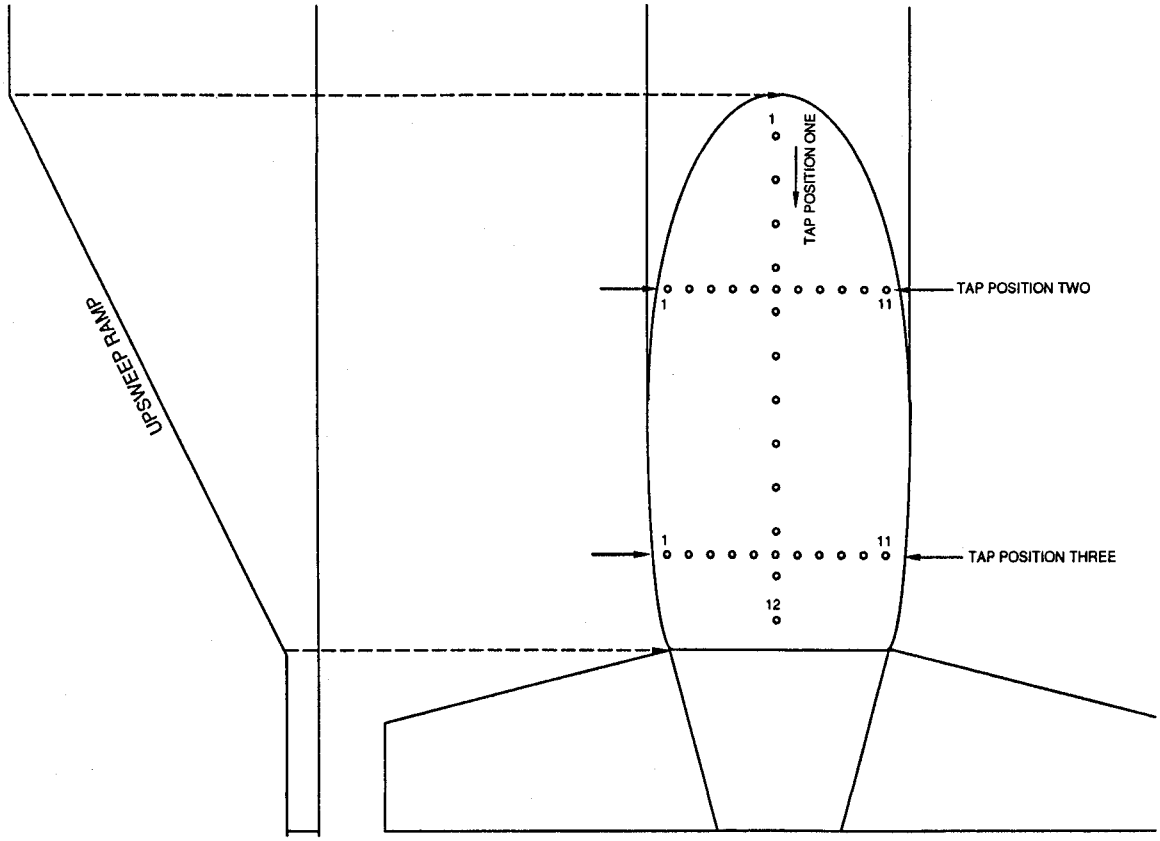

Fig. 9 Pressure tap spatial locations on upswept base of fuselage.

Additional information was derived from the five-hole probe data set, including the crossflow kinetic energy, vorticity, total pressure, and static pressure. The crossflow kinetic energy and vorticity are shown in Fig. 7. The total pressure and static pressure are shown in Fig. 8. The flowfield is symmetric, therefore, only half the crossflow plane is shown for the sake of clarity. All velocities are nondimensionalized by the reference freestream velocity. The crossflow kinetic energy is nondimensionalized by the freestream kinetic energy. The static pressure and total pressure values are nondimensionalized by their reference values. The vorticity contours are nondimensionalized by the freestream velocity, and a length scale equal to the diameter of the model fuselage. Looking at the total pressure isolines (Fig. 8), we see the loss of total pressure in the wake. The isolines represent the deficit of total pressure between the local value and the reference value in the settling chamber expressed in terms of reference dynamic pressure. As such, if no losses occur, the isoline value will equal zero, and if losses occur then the according value is positive since the local total pressure is usually less than the reference total pressure due to the energy lost in the wake. Similarly, looking at the crossflow kinetic energy (Fig. 7), the energy lost in the wake can be seen. It varies radially from the center of the core with a peak value corresponding to the outermost point of the core radius; the higher the crossflow kinetic energy, the higher the wake energy deficit resulting in increased losses due to vortex drag. Finally, the vorticity isolines (Fig. 7), show that the vorticity field is distributed radially about the center of the vortex with the highest concentration of vorticity confined almost exclusively to the central core region.

As an additional note, the velocity in the crossflow plane was found to be very similar to that of a simple point vortex with a quadratic rotational core function. The remarkable correlation between the quadratic core vortex and the measured data is shown later in this article. Additionally, using an analytical formulation, the circulation of the shed vortices is calculated.

Base Pressure Measurements

Base pressure measurements were done at three Reynolds numbers: 8.3×10^4, 1.66×10^5, and 2.37×10^5. The test runs were in the incompressible subsonic range. Many base pressure runs were recorded and representative results are being presented in this article. Again, all of the work presented was done at a fixed fuselage angle of attack parallel to the oncoming freestream.

The base pressure measurements are organized into three groups by spatial position on the fuselage (Fig. 9). Group one represents the measurements taken at 12 pressure taps located along the axial center of the upsweep starting at the end of the cylindrical portion of the fuselage and ending on the beaver tail or top portion of the horizontal stabilizer. In general, the pressure seems to increase along the fuselage in the direction of the freestream. This trend is demonstrated by the other tap positions that plot the pressure distributions across the upsweep spanwise. Figure 10 shows the results of the pressure measurements.

Group two represents the 11 pressure taps located at the top portion of the upsweep, away from the horizontal stabilizer; group three is the 11 pressure taps located considerably closer to the horizontal stabilizer, as depicted in Fig. 9. The pressure along group three is clearly higher than along group two. In both groups, a local pressure maximum is found at the center of the base ramp, and the minimum are located at the base ramp fuselage intersection. This pressure variation is due to the flowfield pressure variations created by the shed vortices.

Geometric nonuniformities in the pressure taps are the major sources of error in this type of experiment, barring errors due to the pressure transducer. Accordingly, great care was taken to make the pressure taps with sharp-edged holes, per-

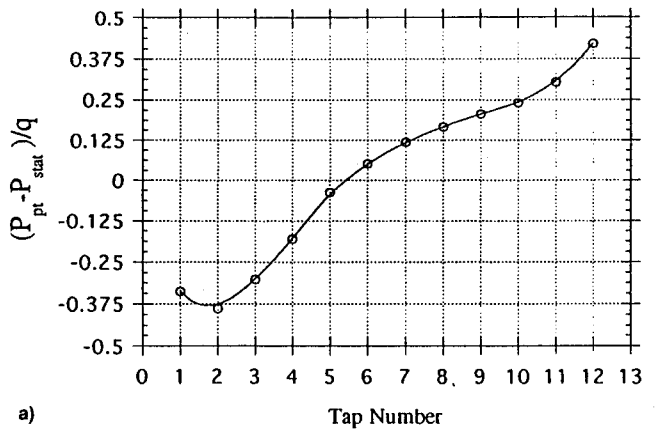

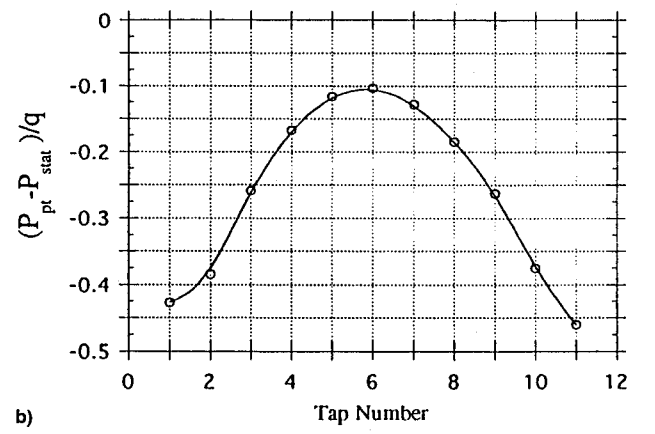

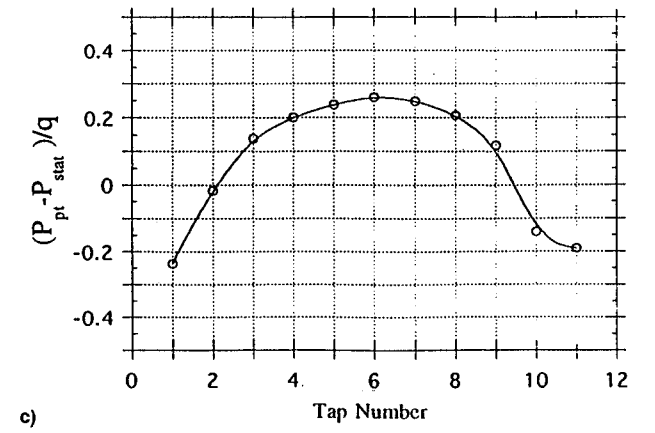

Fig. 10 Pressure tap measurements along position a) one, b) two, and c) three (Re = 2.37 × 10^5).

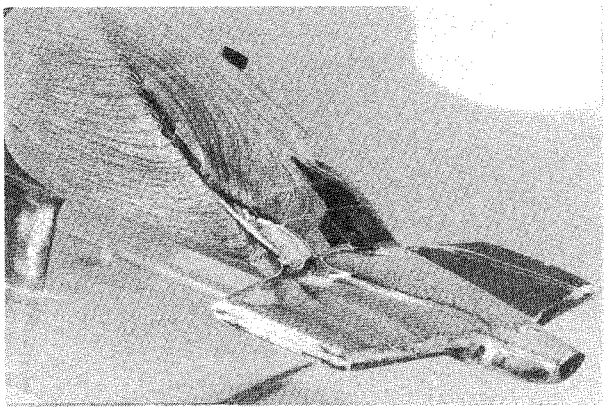

Fig. 11 Oil flow visualization showing the strong separation line (Re = 2.37 × 10^5).

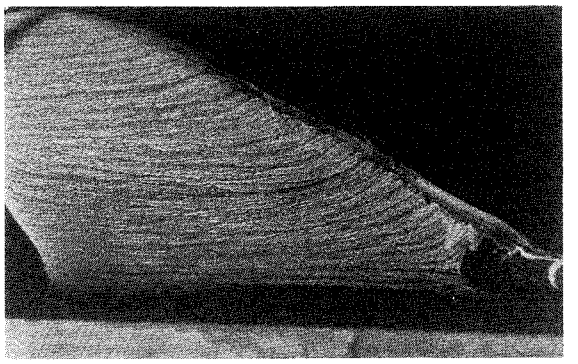

Fig. 12 Oil flow visualization on the upswept fuselage base (Re = 2.37 × 10^5).

pendicular to the fuselage surface, and free from burrs. The upsweep ramp was made of balsa wood smoothly finished with black lacquer. The pressure taps were fabricated from plastic tubing and epoxy resin.

The pressure transducer was similar to the one used for the five-hole probe measurements. The specifications for the transducer state that there is only a 0.5% variation on the best straight line with a very limited hysteresis of 0.5% of the total pressure excursion. The specifications were verified by a calibration involving a first-order, least-squares fit to the data. The total error, including the curve fit, resulted in the specified accuracy with a confidence level of (1:25).

Base Oil Flow Visualization

Visualizations were carried out at a Reynolds number of 2.37 × 10^4. The visualization fluid was a mixture of oil, talc, oleic acid, and titanium oxide such that the consistency was capable of flowing freely without being excessively distorted by gravitational effects. Adjustment of the proportions was necessary, as usual, to optimize the results. Many different tests were completed and selected results have been presented in Figs. 11 and 12.

The technique used is quite simple. The visualization fluid was applied to the model prior to the test, then the tunnel was activated and accelerated to the desired test speed. During the acceleration process and the subsequent tunnel run, the flow of the visualization fluid was carefully observed. After about 10–15 tests, the general trend of the flowfield could be anticipated; the proportions and the application of the visualization fluid could be adjusted accordingly to improve the desired results.

When dealing with oil flow visualization, it is important to stress the high level of inaccuracy associated with the technique. It is very difficult to try to quantify the errors, because the results from a oil flow visualization are hard to quantify. The indisputable advantage of the technique is that it gives an understanding, at least in a general integrated sense, of the trends occurring on the surface of a body, such as separation or attachment lines.

Most notable in Figs. 11 and 12 is the strong separation line along the position where the base ramp attaches to the fuselage. Corresponding to the results of Peake,[1] the separation line is of the bifurcation type. However, the separation line seems to split into two separation lines partially along the upsweep. As such, it represents a fairly mysterious structure, because Y-shaped separation lines are far from the ordinary type expected. This structure, however, is probably due to the beaver-tail formation of the aft fuselage. Additionally, the surface flow from the forward section of the fuselage is seen to travel along the upsweep and separate from the fuselage at the lower portion of the bifurcated separation line, or simply separate at the point of highest curvature along the upsweep-fuselage joint. Figure 11 shows the separation line quite clearly.

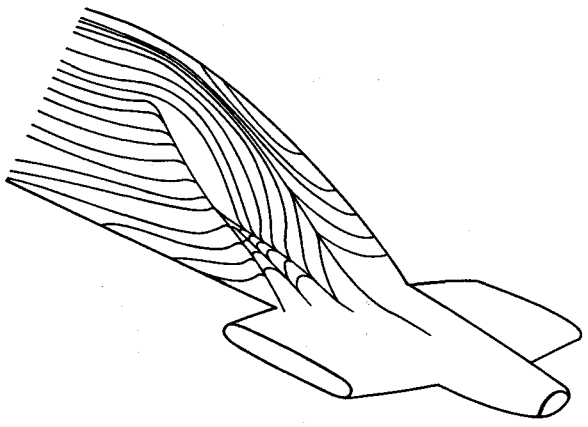

Fig. 13 Interpretation of the surface flow steamlines from the oil flow visualization experiments ($Re = 2.37 \times 10^5$).

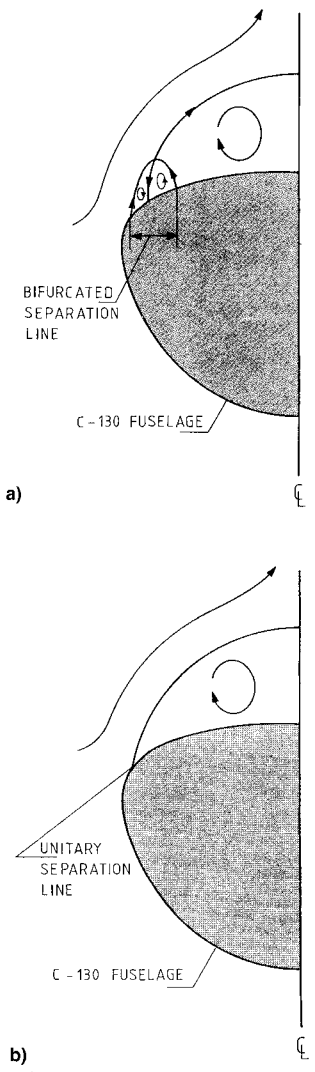

Fig. 14 Possible crossflow velocity field just above fuselage surface based on surface flow streamlines at two axial stations. x/D = a) 1.48 and b) 0.84.

Figure 13 shows an interpretation of the surface flow streamlines corresponding to the mathematical rules of surface topology and linear stability analysis.[8] The zone inside the bifurcation was observed as a region of reversed flow, as such it gives rise to the present interpretation. It is of considerable interest to look at the flow in the crossflow plane just above the fuselage surface. Figure 14 depicts one possible crossflow field, although one should note that the crossflow velocity field is not uniquely determined by the surface flow topology, and other velocity fields in the crossflow plane above the fuselage surface are possible.

Analytical Development and Results

The concept of a rotational vortex core becomes indispensable when considering physical vortex problems. From the theory of classical inviscid aerodynamics it is known that the velocity distribution induced by a vortex filament of strength Γ is governed by the familiar Biot-Savart Law[9]

$$v = -\frac{\Gamma}{4\pi}\int_\gamma \frac{\boldsymbol{r} \times d\boldsymbol{s}(\gamma)}{|\boldsymbol{r}|^3} \tag{1}$$

with the assumptions that the fluid is unbounded, at rest at infinity, without interior boundaries, and with zero vorticity at all points of the fluid not on the vortex filament itself.

In general, vortex filament dynamics have been analyzed by integrating the Biot-Savart law [Eq. (1)], over the entire filament, where the filament is treated as being of finite strength and infinitesimal cross section. The logarithmic singularity that occurs in the coreless self-induced velocity calculation[10,11] associated with the local curvature of the filament is avoided by stopping the integral at a cutoff distance on either side of the point of evaluation. The correct choice for the cutoff distance is obtained from an asymptotic analysis that gives the result in terms of the local core size and the total energy content of the core.[10,11]

Equation (2) is a modified form of the Biot-Savart law[12] that artificially accounts for the effects of a rotational vortex core by including a smoothing function that removes the filament singularity and attenuates the near-field self-induced velocity:

$$v = -\frac{\Gamma}{4\pi}\int_\gamma \frac{\boldsymbol{r} \times d\boldsymbol{s}(\gamma)}{(r^2 + r_c^2)^{3/2}} \tag{2}$$

The constant core radius r_c effectively spreads the vorticity across a finite area and removes the velocity singularity on the filament itself. This particular core treatment, in addition to being functionally simple, results in an algebraic decay of the core effect with radial distance from the center of the vortex, and is noted as one of the earliest core treatments described in the literature.[13] Integrating Eq. (2) along an infinite straight line results in the following expression for swirl velocity:

$$v_\theta = -\frac{\Gamma}{2\pi}\frac{r}{r^2 + r_c^2}\hat{e}_\theta \tag{3}$$

In the limit as r_c approaches zero, Eq. (3) reduces to the potential vortex result:

$$v_\theta = -(\Gamma/2\pi r)\hat{e}_\theta \tag{4}$$

Note that the addition of the core radius to the Biot-Savart law results in a flowfield that is truly everywhere rotational, and therefore can no longer rigorously be considered a potential flow. The addition of a core spreads the vorticity over an infinite volume, although it is most highly concentrated in the vortex near field. The vorticity generated by the two-dimensional vortex of Eq. (3) is given in the following equation; where vorticity decay occurs as $1/r^4$:

$$\omega = \frac{-\Gamma}{\pi}\frac{r_c^2}{(r^2 + r_c^2)^2} \tag{5}$$

The reader is urged to keep in mind that the vortex core, as described, is a mathematical fabrication that artificially represents real flow effects. Different core functions can be

chosen and, as such, each core manifests itself differently by changing the velocity and vorticity fields accordingly.

Equation (3) can be rewritten as

$$v_\theta = \frac{\Gamma}{2\pi r}\left[\frac{r^2}{(r^2 + r_c^2)}\right]\hat{e}_\theta \tag{6}$$

This is sometimes referred to as a two-dimensional "vorton."

A simple analytical model for the flow in the afterbody crossflow plane, called the double vorton model (DVM), was constructed in order to model the velocity and vorticity fields in the crossflow plane and facilitate physical understanding. The DVM model is composed of two vortons of opposite sign located colinearly in the crossflow plane. Using local cylindrical polar coordinates, a vorton is centered on each vortex center of the two symmetric sides of the afterbody wake. The vortex center position and core size are taken from the experimental measurements. The closed form expression for DVM velocity in a crossflow plane is quite lengthy, due to the direction cosines needed, yet it is simple to evaluate. For simplicity, the DVM velocity is given for the swirl velocity induced on the infinite line passing through the vortex centers of both vortons, parallel to the horizontal stabilizer tail plane:

$$v_\theta = \frac{\Gamma}{2\pi}\left(\left\{\frac{(r + L/2)}{[(r + L/2)^2 + r_c^2]}\right\} - \left\{\frac{(r - L/2)}{[(r - L/2)^2 + r_c^2]}\right\}\right)\hat{e}_\theta \tag{7}$$

In Eq. (7), the circulation Γ is constant. The core radius is constant for both vortices. The parameter L is the distance between the vortex centers. The circulation can be determined one of two ways. It can be obtained directly from the velocity measurements, using the experimental grid as a numerical grid, and evaluating the circulation directly, or the DVM profile can be parametrically adjusted as a function of the circulation until the DVM and measured velocity fields coincide.

All the parameters mentioned, Γ, r_c, and L, can be determined with a few horizontal five-hole probe traverses through the near-center position of both vortices. As such, the DVM model is not only analytically simple, it also requires minimal measurements. Figure 15 shows the remarkable agreement between the DVM model and the measured values. In Fig. 15 notice how the structure and the shape of the crossflow velocity field are accurately modeled by the DVM model. Figure 15 also shows a comparison between the interpolated vorticity from the measurement grid, and the vorticity calculated from the DVM model.

Beyond making available a novel tool for the evaluation of vortex flows, the DVM model offers insight into the physics of the afterbody vortex. The vortex core has the same shape as the quadratic core, therefore, it is very smooth without severe velocity gradients. The vorticity drops off as $1/r^4$, demonstrating that most of the vorticity is confined to the core region. The vorticity distribution is radially symmetric about the core. The vortex self-induced velocity is probably quite low due to the large core radius.

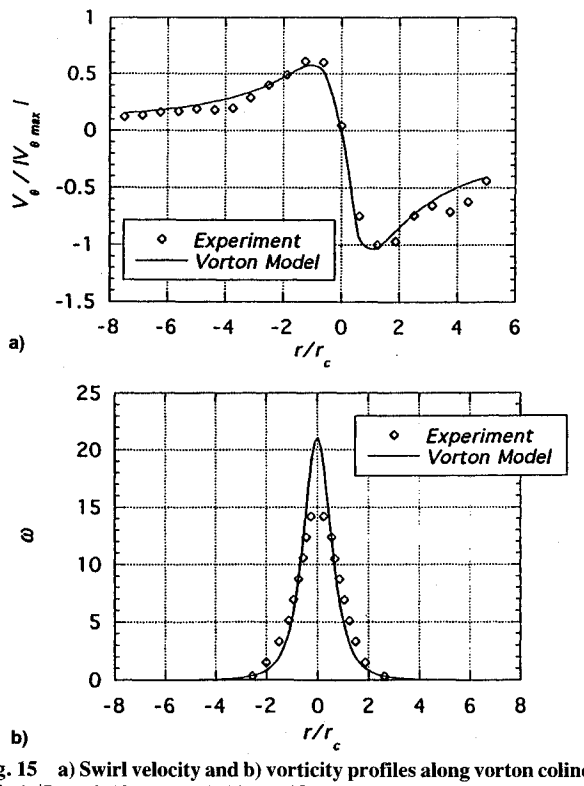

Fig. 15 a) Swirl velocity and b) vorticity profiles along vorton colinear axis (x/D = 2.12, Re = 1.66 × 10^5).

Conclusions

The present work has described the experimental and empirically-based analytical analysis of the flowfield about a fuselage upswept afterbody in a subsonic incompressible flow. The major results are as follows:

1) Experimental measurements have been made in order to verify the flowfield structure about an upswept afterbody.

2) The axial position of the wake vortices has been determined as they convect with the freestream. This phenomena, as well as the wake formation does not seem to have a strong correlation with local Reynolds number. The pressure variations on the upswept base of the fuselage have been measured and correlate with the other data acquired. The surface flow on the base ramp has been documented, and a crossflow field has been postulated in accordance with the surface flow.

3) A simple analytical model for the flow in the crossflow plane has been developed based on the experimental data.

Acknowledgments

This work was partially supported by a U.S. Air Force Fluid Dynamics Fellowship. The authors would like to thank the support staff at the von Kármán Institute for Fluid Dynamics without which this work would have been impossible. Additional thanks are due to the undergraduate laboratory trainees, A. Bonfiglioli and H. Vollebregt, whose time and devotion to the wind-tunnel labs at the VKI is greatly appreciated.

References

[1]Peake, D. J., "The Flows About Upswept Rear Fuselages of Typical Cargo Aircraft," *National Aeronautical Establishment Bulletin*, NRC QUA. BULL DME/NAE, National Research Council of Canada, Vol. 3, 1968.

[2]Tsuboi, K., Shirayama, S., Oana, M., and Kuwahar, K., "Computational Study of the Effect of Base Slant," *Supercomputer Applications in Automotive Research and Engineering Development*, Cray Research, Minneapolis, MN, 1988, pp. 257–272.

[3]Ashley, H., and Landahl, M., *Aerodynamics of Wings and Bodies*, Dover, NY, 1965, pp. 135–137.

[4]Thomas, A. S. W., "Aircraft Drag Reduction Technology—A Summary," *Aircraft Drag Prediction and Reduction*, AGARD Rept. 723, July 1985.

[5]Treaster, A. L., and Yocum, A. M., "The Calibration and Application of Five-Hole Probes," Pennsylvania State Univ., TM 78-10, State College, PA, Jan. 1978.

[6]Samet, M., and Einav, S., "Directional Pressure Probes," *Review of Scientific Instruments*, Vol. 55, No. 4, 1984, pp. 582–588.

[7]Caudron, F., "Vortex Strake Interaction and Its Application to the Drag Reduction of Upswept Rear Fuselage," The von Kármán Inst. for Fluid Mechanics, VKI PR 1990-27, Rhode-Saint-Genese,

Belgium, June 1990.

[8]Degrez, G., "Flowfield Kinematics: Streamlines and Skin Friction Lines," *Course Notes on Three-Dimensional Boundary Layer Theory*, The von Kármán Inst. for Fluid Dynamics, Rhode-Saint-Genese, Belgium, 1992, pp. 2–10.

[9]Batchelor, G. K., *An Introduction To Fluid Mechanics*, Cambridge Univ. Press, Cambridge, England, UK, 1967, pp. 507–517.

[10]Bliss, D. B., *The Dynamics of Curved Rotational Vortex Lines*, M.S. Thesis, Massachusetts Inst. of Technology, Cambridge, MA, 1970.

[11]Widnall, S. E., Bliss, D. B., and Zalay, A., "Theoretical and Experimental Study of the Stability of a Vortex Pair," *Aircraft Wake Turbulence and Its Detection*, Plenum Press, NY, 1971, pp. 305–338.

[12]Miller, W. O., *Analytical/Numerical Matching and Periodic Inversion: Two Advances in Free Wake Analysis*, Ph.D. Dissertation, Duke Univ., Durham, NC, 1990.

[13]Rosenhead, L., "The Spread of Vorticity in the Wake Behind a Cylinder," *Proceedings of the Royal Society of London*, Ser. A-127, 1930, pp. 590–612.

[14]Britcher, C. P., and Alcorn, C. W., "Interference-Free Measurements of the Subsonic Aerodynamics of Slanted-Base Ogive Cylinders,"*AIAA Journal*, Vol. 29, No. 4, 1991, pp. 520–525.